RSC Advances

PAPER

View Article Online
View Journal | View Issue

Cite this: *RSC Adv.*, 2026, **16**, 14049

Temperature-triggered microfluidic fabrication of monodisperse organic particles *via* LCST-mediated phase transition

Keita Tanita, [a] Ryuju Suzuki, [b] Hitoshi Kasai, [c] Mao Fukuyama, [c] Akihide Hibara [d] and Takayuki Ishizaka *[a]

Received 9th November 2025
Accepted 9th March 2026

DOI: 10.1039/d5ra08639f

rsc.li/rsc-advances

We report a microfluidic strategy for fabricating monodisperse organic particles by exploiting temperature-controlled miscibility in mixed solvents exhibiting lower critical solution temperature (LCST) behavior. In a water–diethylene glycol monohexyl ether (C6E2) system, phase separation at elevated temperatures enables controlled generation of monodisperse droplets, which subsequently reprecipitate into particles upon cooling to the miscible state. As a result, poly(vinyl alcohol) microparticles with a coefficient of variation below 9% were successfully obtained. This LCST-driven microfluidic approach offers a general platform for producing highly uniform particles from both polymeric and low-molecular-weight organic compounds.

In recent years, organic particles, defined as solid particles consisting of polymers or low-molecular-weight compounds, have been essential in many applications, such as photocatalysts,[1] standards for size calibration, medicines,[2,3] and other composite materials.[4,5] Since the chemical and physical properties of particles depend on their size,[2,4] it is necessary to fabricate monodisperse particles with controlled sizes.

Emulsion and miniemulsion polymerization are widely used as the heterogeneous processes for the fabrication of monodisperse organic particles composed of polymers.[6,7] Both methods are formulated with a hydrophobic monomer, a surfactant and water. In particular, miniemulsion polymerization gives one monodisperse polymer particle from one monodisperse monomer droplet.[7] However, applicable monomers are limited only to typical compounds with vinyl groups. Similarly, top-down and bottom-up methods have been proposed for the fabrication of organic particles composed of low-molecular-weight compounds.[8,9] Although many bottom-up methods that utilize difference in solubility have been developed, there is no method for producing monodisperse particles. It is difficult to homogenize the entire system using simple mixing in batch or flow systems. If monodisperse droplets dissolving target compounds are generated in poor solvent and one droplet produces one particle, it is possible to establish a new method for fabricating monodisperse organic particles that can be applied to both polymers and low-molecular-weight compounds.

In order to realize the strategy, we focused on lower critical solution temperature (LCST)-type mixed solvents with liquid–liquid two-phase at high temperatures and one liquid phase at low temperatures (Fig. 1A).[10–13] The mixture of water and glycol ethers (water-CnEm),[10–12] and water-amine[13] were well known. Their unique behaviour derives from the competition between the incompatibility of water and hydrophobic parts of solvent, and the hydrogen bonding between water and hydroxyl groups of solvent.[11,14] These solvents are also commonly used for the extraction and separation of salts and target compounds through phase transitions.[15] By utilizing these solvent systems, it was proposed to separate the droplet formation step and the particle precipitation step by temperature clearly (Fig. 1B). In

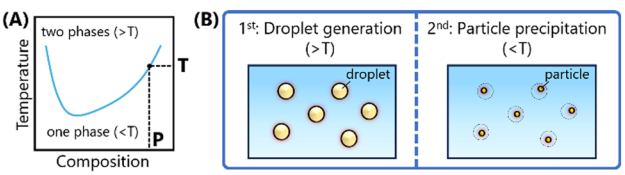

Fig. 1 Schematic illustration of this study. (A) Typical phase diagram of an LCST-type binary mixture. The mixed solvent (composition P) is in two phases above the critical temperature T, and in one phase below the T. (B) The strategy of this study. The 1st step: monodisperse droplets in which the target compound is dissolved are generated above the T. The 2nd step: the droplets miscible with the poor solvent below T, and target compounds precipitated in the mixed solvent.

[a]*Research Institute for Chemical Process Technology, National Institute of Advanced Industrial Science and Technology (AIST), 4-2-1 Nigatake, Miyagino-ku, Sendai, Miyagi 983-8551, Japan. E-mail: t-ishizaka@aist.go.jp*

[b]*National Institute of Technology, Sendai College, 48 Nodayama, Medeshima-Shiote, Natori, Miyagi 981-1239, Japan*

[c]*Institute of Multidisciplinary Research for Advanced Materials, Tohoku University, 2-1-1 Katahira, Aoba-ku, Sendai, Miyagi 980-8577, Japan*

[d]*Department of Chemistry, School of Science, Tokyo Institute of Technology, 2-12-1 Ookayama, Meguro-ku, Tokyo 152-8551, Japan*

this paper, we report the results of precipitation from emulsion droplets containing poly(vinyl alcohol) (PVA) caused by temperature-dependent miscibility, as the first model of this research. PVA is a water-soluble polymer, and their particles are utilized to some applications (*e.g.* embolic particles,[16,17] matrix for enzyme immobilization,[18] and drug carriers[19,20]). In the water-diethylene glycol monohexyl ether (C6E2) binary mixture system, water is a good solvent and C6E2 is a poor solvent for PVA, respectively. The continuous generation of monodisperse droplets was performed by utilizing polydimethylsiloxane (PDMS)-based microfluidic devices. Microfluidics possesses the ability to control droplet sizes by changing conditions, such as microchannel characteristic size and flow rate.[21,22] It is able to generate W/O type emulsions and O/W type emulsions by controlling the wettability of PDMS with surface modification.[23]

First, the compatibility of PDMS with water-C6E2 binary mixture was confirmed for application of PDMS-based microfluidic devices. Swelling changes the cross-sectional area of the channel and causes the microfluidic device to collapse. Solvent compatibility of PDMS is classified by the degree of swelling that is expressed by the swelling ratio $(S): S = D/D_0$, where D is the length of a PDMS sheet after immersion in solvent for 24 hours and D_0 is the length of the dry PDMS sheet.[24] The swelling ratio of PDMS in C6E2 was exceedingly low, and there was almost no change in the length of PDMS sheets after immersing in C6E2 for 24 hours ($S = 1.00$, Fig. S1). In the previous classification,[24] it should be possible to generate the droplets in these solvents system with PDMS-based microfluidic device.

As with generally PDMS-based microfluidics, the dispersed phase needed to be non-wetting with PDMS to avoid adhesion on device walls.[25] In this experiment, we found a reversal of wettability to the PDMS sheet as the temperature increased (Fig. 2A). When a droplet composed of a water-rich phase (W) was dropped on a PDMS sheet in a C6E2-rich phase (O) at 25 °C, the contact angle of 62.8° was calculated by $\theta/2$ method. This result showed that the dispersed phase wetted the walls of the microdevices fabricated by PDMS. As the temperature was gradually increased, the wettability reversed at around 40 °C, and the contact angles finally reached 124.6° at 75 °C. There is a qualitative rule for the liquid–liquid interfacial tension related to the mutual solubility: smaller mutual solubility gives greater interfacial tension.[26] For a water-C6E2 binary mixture system with LCST-phase transition, increasing temperature leads to increasing the liquid–liquid interfacial tension.

As shown in Fig. S2, focusing on the composition of C6E2 with temperature change from 25 to 75 °C, the aqueous phase did not change significantly from 1.76 to 0.98 wt%.[27] On the other hand, the composition of C6E2 in the organic phase changed from 52.1 to 77.4 wt%.[27] The relative decrease in surface free energy between the organic phase and PDMS may have led to a reversal of the interfacial tension balance (Fig. 2B). The mixed solvent system in this paper suggested that the ratio of the degree of solvent mixing has a qualitative relation to the contact angle. The wetting transitions observed in this study are consistent with the prediction of the critical point wetting theory,[28] and the contact angle on a PDMS substrate is expected to be zero near their lower critical solution temperature. It was

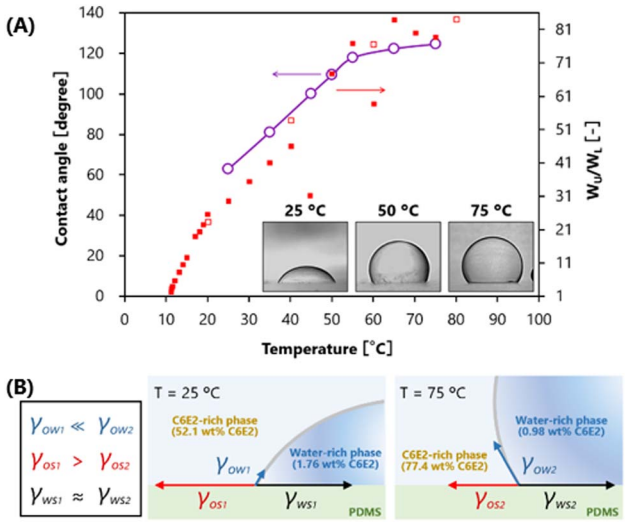

Fig. 2 (A) Temperature dependence of the wettability of water-C6E2 binary mixture on a PDMS surface. Solid line: contact angles formed by the water-rich phase on a PDMS surface ($n = 3$). The contact angle formed by a droplet varied with temperature. The ratio of the degree of solvent mixing; empty symbols (ref. 13); filled symbols (ref. 27). (B) Schematic illustration of wettability change controlled by the temperature-dependent interfacial tension balance. γ_{ow}: liquid–liquid interfacial tension; γ_{os}: surface free energy between the organic phase and PDMS; γ_{ws}: surface free energy between the aqueous phase and PDMS.

suggested that W/O emulsion droplets did not contact with wall surfaces under the liquid–liquid two-phase state at high temperature.

Our microfluidic device, designed for monodisperse droplet generation, included a flow-focusing junction where one dispersed phase-channel intersects two continuous phase-channels. The microchannel pattern was transferred onto a PDMS substrate by a microchannel mold, and then the PDMS substrate with the imprinted channel was bonded to another smooth PDMS sheet. The prepared microchannel was enclosed in a housing (Fig. S3). Microchannel molds and housings were printed by 3D printer. The inside of the microdevice was heated above a critical temperature, and the generated droplets were observed with a high-speed camera (Fig. S4).

It was investigated whether W/O droplets could be continuously generated in our microfluidic system. The dispersed and continuous phases used water and a mixture of water and C6E2 (19 : 80 (v/v)), respectively. The disperse phase was supplied to the microfluidic device at five sets of flow rates ($Q_d = 1.0$, 2.0, 3.0, 4.0 and 5.0 μL min^{-1}), and the flow ratio of dispersed phase to continuous phase was fixed at 1 : 99 in all conditions. W/O droplets were successfully generated in the microfluidic device under 80 °C and all collected solutions formed a homogeneous phase in all conditions at room temperature. These results indicated that droplets transitioned from immiscible to miscible by controlled temperature. Focusing on the droplets generation time, it is clear that larger total flow rate gave shorter interval of generation time (Fig. 3A). The increase in the fluid velocity led higher shear stress at the interface between the two

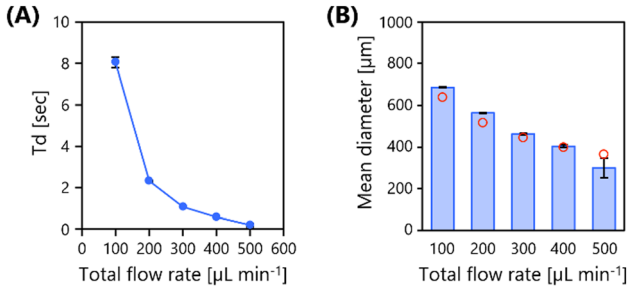

Fig. 3 (A) Influence of the total flow rate on the droplet generation time. (B) Influence of the total flow rate on the droplets size. The flow ratio of dispersed phase to continuous phase was fixed at 1 : 99 in all conditions. These results are indicated as the mean ± standard error (n = 10). Empty symbols: the predicted droplet sizes obtained from eqn (18) in ref. 29.

phases, resulting in faster droplet formation. The diameter of the generated droplets is smaller in size with increasing the flow rate (Fig. 3B). The mean diameter of the generated droplets also correlated well with predicted values calculated from the equation in reference (Table S1).[29] The monodispersity of the droplets was evaluated by the coefficient of variation (CV), which is defined as CV = σ/μ where σ and μ are standard deviation and mean of population, respectively. The square of the CV value corresponds to the polydispersity index (PDI). In the case of Q_d = 1.0, 2.0, 3.0 and 4.0 μL min^{-1}, the CV values measured were <2% much lower than the typical criterion of 10% for monodispersity of particle sizes. In contrast, the CV value at Q_d = 5.0 μL min^{-1} was over the typical criterion, suggesting that a change in the droplet generation mode occurred with an increase in the total flow rate.

Monodisperse PVA particles were fabricated from monodisperse droplets of PVA aqueous solution. The continuous phase is a binary mixture of water and C6E2 in the ratio of 19 : 80 (v/v), as in the droplet generation experiment, while a 3 wt% PVA aqueous solution was supplied as the dispersed phase solution. The mean diameter of the generated droplets of PVA aqueous solution was 343.7 μm, and their CV value was 4.0%. After collection in a sample bottle, it was visually observed that PVA precipitated in the mixed solvents. The obtained PVA precipitates were spherical with a mean diameter of 98.9 μm; the CV value was 8.9%, confirming that the fabricated PVA particles were highly monodispersed (Fig. 4A). To clarify the correlation between the size distribution of droplets and obtained corresponding particles, we next fabricated PVA particles from droplets with a large variation in size. The polydisperse droplets were generated by simple stirring (1500 rpm) of the continuous phase and the dispersed phase above the critical temperature. The shear force of stirring generates a large number of small droplets, but their sizes are not controlled. The obtained PVA precipitates were spherical particles with a mean diameter of 20.0 μm, whereas the CV value was 80.0%. It is suggested that the size distribution of obtained particles was due to the polydispersity of droplet sizes (Fig. 4B). In contrast, when a simple stirring was applied at room temperature, the formation of aggregates was observed immediately in the mixed solvent. The SEM image showed that thread-like aggregates of less than 10 μm were assembled together and large agglomeration was formed. It is possible that these PVA aggregates precipitated earlier than shearing for droplets generation under room temperature. It was clear that the "phase separation state above the critical temperature" and the "generation of monodisperse droplets" were the key to fabrication of monodisperse particles in our system.

If this method is restricted to the water-C6E2 binary system, the organic compounds applicable to this method would be severely limited. Our strategy was able to be applied to not only binary systems, but also multi-component mixtures of solvents. A ternary system including binary mixture with temperature-dependent phase transition was searched by simulation for calculating thermodynamic properties of liquid mixtures. By

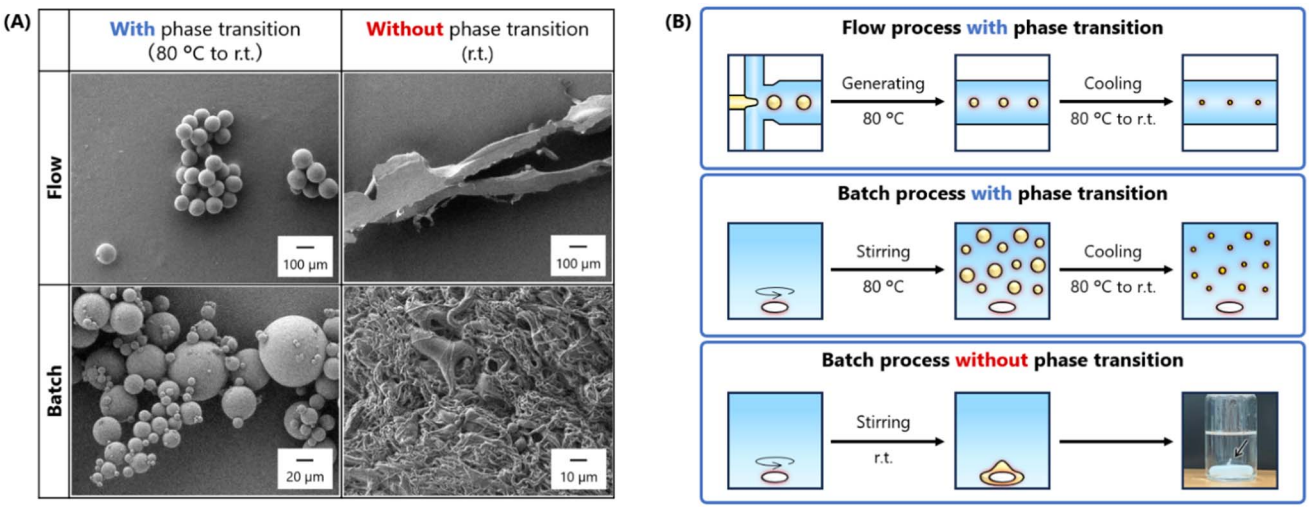

Fig. 4 (A) SEM images of PVA precipitates; PVA precipitated in tube *via* monodisperse droplet states (top-left). PVA precipitated in the microdevice without *via* droplet states (top-right). PVA precipitated in bottle stirred by stirrer bar *via* droplet states (bottom-left). PVA precipitated on the stirrer bar immediately after injection into the poor solvent (bottom-right). (B) Mechanism of PVA precipitation.

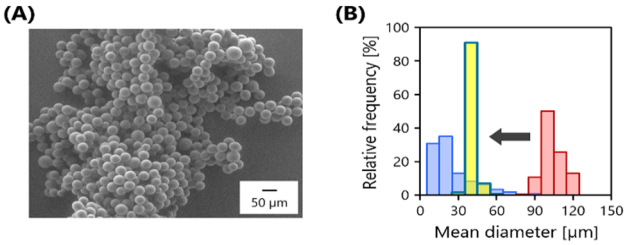

Fig. 5 (A) SEM image of PVA microparticles fabricated by mold with a narrow channel width. (B) Size distribution histogram of PVA particles with different fabrication method. Simple stirring by batch process (blue); using microfluidic device in above section (red); using microfluidic device with narrow pathway (yellow).

utilizing a ternary system of water plus ethylene glycol monobutyl ether plus 1-hexanol, monodisperse microparticles composed of sodium alginate or PVA, were successfully prepared respectively (Fig. S5 and S6). The utilization of multicomponent phase diagram is needed to fabricate particles of a wide range of compounds (*e.g.*, polymers, small molecules, and biocompatible molecules *etc.*) from W/O or O/W emulsions.

The droplet size is determined by experimental parameters like channel geometry, dimensions, interface tension, two-phase flow rate ratio, flow velocity ratio, and viscosity.[30] Although it was generally convenient to control the flow rate ratio to change the size, the flow ratio could not be changed for maintain the composition of LCST state. A shift in solvent composition may result in LCST-phase transition not occurring. To fabricate smaller PVA particles, we improved geometrical parameters of microchannels to generate smaller droplets. The new mold possesses a narrow continuous phase-channel which is equal to 0.5 times the previous channel width (Fig. S7).

The mean diameter of the observed W/O droplets was 167.8 μm, which was about 0.49 times smaller than that observed with using the wider channel. The size distribution was also narrow and classified monodisperse, as shown in their CV value (6.1%) (Fig. S8). The SEM images showed that obtained PVA particles were spherical shape, with a mean diameter of 35.9 μm (Fig. 5A). In addition, size distribution profile showed that smaller monodisperse particles were successfully fabricated (Fig. 5B). It was clear that the "the size-control of generated droplets" was a key to controlling the size of obtained particles in our system.

In this study, we proposed an innovative microfluidic system using mixed solvents with temperature-dependent miscibility for the fabrication of monodisperse particles. The investigation of swelling ratio and contact angles in a water-C6E2 binary mixture system with LCST-phase transition, showed solvent stability of PDMS-based microfluidic devices. Monodisperse droplets were continuously generated under phase separation state above the critical temperature, and the phase changed from immiscible to miscible with decreasing temperature. Monodisperse PVA microparticles were successfully fabricated *via* phase transition-induced solvent dissolution from droplets into the continuous phase. In future, this approach, which utilizes LCST-phase transition of mixed solvent, could be applied to fabrication of monodisperse particles composed of polymers or low-molecular-weight compounds.

Conflicts of interest

There are no conflicts of interest to declare.

Data availability

The data supporting this article have been included as part of the supplementary information (SI). Supplementary information is available. See DOI: https://doi.org/10.1039/d5ra08639f.

Acknowledgements

A part of this study is based on the results obtained from project JPNP19004, commissioned by the New Energy and Industrial Technology Development Organization (NEDO), Japan.

Notes and references

1 Y. Shiraishi, T. Takii, T. Hagi, S. Mori, Y. Kofuji, Y. Kitagawa, S. Tanaka, S. Ichikawa and T. Hirai, *Nat. Mater.*, 2019, **18**, 985–993.
2 Q. Xu, M. Hashimoto, T. T. Dang, T. Hoare, D. S. Kohane, G. M. Whitesides, R. Langer and D. G. Anderson, *Small*, 2009, **5**, 1575–1581.
3 K. Tanita, Y. Koseki, S. Kumar, F. Taemaitree, A. Mizutani, H. Nakatsuji, R. Suzuki, A. T. N. Dao, F. Fujishima, H. Tada, T. Ishida, K. Saijo, C. Ishioka and H. Kasai, *Nanoscale*, 2024, **16**, 15256–15264.
4 S. Homaeigohar, R. Kabir and M. Elbahri, *Sci. Rep.*, 2020, **10**, 5191.
5 Y. He, J. Zhang, Y. Cai and L. Yi, *Prog. Org. Coat.*, 2021, **159**, 106403.
6 C. S. Chern, *Prog. Polym. Sci.*, 2006, **31**, 443–486.
7 M. Antonietti and K. Landfester, *Prog. Plym. Sci.*, 2002, **27**, 689–757.
8 Z. H. Loh, A. K. Samanta and P. W. S. Heng, *Asian J. Pharm. Sci.*, 2015, **10**, 255–274.
9 B. Sinha, R. H. Müller and J. P. Möschwitzer, *Int. J. Pharm.*, 2013, **453**, 126–141.
10 H. H. Lai and L. J. Chen, *J. Chem. Eng. Data*, 1999, **44**, 251–253.
11 S. P. Christensen, F. A. Donate, T. C. Frank, R. J. LaTulip and L. C. Wilson, *J. Chem. Eng. Data*, 2005, **50**, 869–877.
12 C. Browarzik and D. Browarzik, *Fluid Phase Equilib.*, 2005, **235**, 127–138.
13 F. Pousaneh, O. Edholm and A. Maciolek, *J. Chem. Phys.*, 2016, **145**, 014501.
14 Y. Koga, *J. Phys. Chem.*, 1996, **100**, 5172–5181.
15 D. Nakayama, Y. Mok, M. Noh, J. Park, S. Kang and Y. Lee, *Phys. Chem. Chem. Phys.*, 2014, **16**, 5319–5325.
16 R. Cilliers, Y. Song, E. K. Kohlmeir, A. C. Larson, R. A. Omary and T. J. Meade, *Magn. Reason. Med.*, 2008, **59**, 898–902.
17 Y. Wang, Z. Ren, H. Wu, Y. Cao, B. Yu, H. Cong and Y. Shen, *ACS Appl. Mater. Interfaces*, 2024, **16**, 43283–43301.

18 E. Piacentini, M. Yang and L. Giorno, *J. Membr. Sci.*, 2017, **524**, 79–86.
19 B. Felice, M. P. Prabhakaran, M. Zamani, A. P. Rodriguez and S. Ramakrishna, *Polym. Int.*, 2015, **64**, 1722–1732.
20 D. M. Silva, R. Paleco, D. Traini and V. Sencadas, *Int. J. Pharm.*, 2018, **547**, 114–121.
21 T. Thorsen, R. W. Roberts, F. H. Arnold and S. R. Quake, *Phys. Rev. Lett.*, 2001, **86**, 4163–4166.
22 T. Nisisako, T. Torii and T. Higuchi, *Lab Chip*, 2002, **2**, 24–26.
23 T. Trantidou, Y. Elani, E. Parsons and O. Ces, *Microsyst. Nanoeng.*, 2017, **3**, 16091.
24 J. N. Lee, C. Park and G. M. Whitesides, *Anal. Chem.*, 2003, **75**, 6544–6554.
25 J. Du, N. Ibaseta and P. Guichardon, *Chem. Eng. Res. Des.*, 2020, **159**, 615–627.
26 C. K. Wu and L. J. Chen, *J. Chem. Phys.*, 2005, **123**, 084506.
27 K. H. Lim, J. S. Reckley and D. H. Smith, *J. Colloid Interface Sci.*, 1993, **161**, 465–470.
28 J. W. Cahn, *J. Chem. Phys.*, 1977, **66**, 3667–3672.
29 P. Zhu and L. Wang, *Lab Chip*, 2017, **17**, 34–75.
30 A. Britel, G. Tomagra, P. Apra, V. Varzi, S. Sturari, N. H. Amine, P. Olivero and F. Picollo, *RSC Adv.*, 2024, **14**, 7770–7778.